

Effects of built-in electric field and donor impurity on linear and nonlinear optical properties of wurtzite $In_xGa_{1-x}N$/GaN nanostructures

Xiao-Chen Yang(杨晓晨), Yan Xing(邢雁)
Citation: Chin. Phys. B . 2020, 29(8): 087802 . **doi:** 10.1088/1674-1056/ab9291
Journal homepage: http://cpb.iphy.ac.cn; http://iopscience.iop.org/cpb

What follows is a list of articles you may be interested in

Preparation and photoelectric properties of cadmium sulfide quantum dots

Yue Gu(古月), Libin Tang(唐利斌), Xiaopeng Guo(郭小鹏), Jinzhong Xiang(项金钟), Kar Seng Teng, Shu Ping Lau(刘树平)
Chin. Phys. B . 2019, 28(4): 047803 . **doi:** 10.1088/1674-1056/28/4/047803

SnS_2 quantum dots: Facile synthesis, properties, and applications in ultraviolet photodetector

Yao Li(李尧), Libin Tang(唐利斌), Rujie Li(李汝劼), Jinzhong Xiang(项金钟), Kar Seng Teng, Shu Ping Lau(刘树平)
Chin. Phys. B . 2019, 28(3): 037801 . **doi:** 10.1088/1674-1056/28/3/037801

Quantum frequency down-conversion of single photons at 1552 nm from single InAs quantum dot

Ben Ma(马奔), Si-Hang Wei(魏思航), Ze-Sheng Chen(陈泽升), Xiang-Jun Shang(尚向军), Hai-Qiao Ni(倪海桥), Zhi-Chuan Niu(牛智川)
Chin. Phys. B . 2018, 27(9): 097802 . **doi:** 10.1088/1674-1056/27/9/097802

Magneto-optical properties of self-assembled InAs quantum dots for quantum information processing

Jing Tang(唐静), Xiu-Lai Xu(许秀来)
Chin. Phys. B . 2018, 27(2): 027804 . **doi:** 10.1088/1674-1056/27/2/027804

Temperature-dependent photoluminescence of size-tunable ZnAgInSe quaternary quantum dots

Qi Ding(丁琪), Xiao-Song Zhang(张晓松), Lan Li(李岚), Jian-Ping Xu(徐建萍), Ping Zhou(周平), Xiao-Fei Dong(董晓菲), Ming Yan(晏明)
Chin. Phys. B . 2017, 26(6): 067804 . **doi:** 10.1088/1674-1056/26/6/067804

Effects of built-in electric field and donor impurity on linear and nonlinear optical properties of wurtzite $In_xGa_{1-x}N$/GaN nanostructures*

Xiao-Chen Yang(杨晓晨) and Yan Xing(邢雁)†

School of Physical Science and Technology, Inner Mongolia University, Hohhot 010021, *China*

(Received 8 March 2020; revised manuscript received 4 May 2020; accepted manuscript online 13 May 2020)

The linear and nonlinear optical absorption coefficients (ACs) and refraction index changes (RICs) of 1s–1p, 1p–1d, and 1f–1d transitions are investigated in a wurtzite $In_xGa_{1-x}N$/GaN core–shell quantum dot (CSQD) with donor impurity by using density matrix approach. The effects of built-in electric field (BEF), ternary mixed crystal (TMC), impurity, and CSQD size are studied in detail. The finite element method is used to calculate the ground and excited energy state energy and wave function. The results reveal that the BEF has a great influence on the linear, nonlinear, and total ACs and RICs. The presence of impurity leads the resonant peaks of the ACs and RICs to be blue-shifted for all transitions, especially for 1s–1p transition. It is also found that the resonant peaks of the ACs and RICs present a red shift with In-composition decreasing or core radius increasing. Moreover, the amplitudes of the ACs and RICs are strongly affected by the incident optical intensity. The absorption saturation is more sensitive without the impurity than with the impurity, and the appearance of absorption saturation requires a larger incident optical intensity when considering the BEF.

Keywords: core–shell quantum dot, linear and nonlinear optical properties, impurity, ternary mixed crystal

PACS: 78.67.Hc, 78.20.Ci, 42.65.–k **DOI:** 10.1088/1674-1056/ab9291

1. Introduction

In the last decade, semiconductor nanostructures have attracted the considerable attention due to their great potential applications in opto-electronic devices.[1–11] Among these nanostructures, core–shell quantum dots (CSQDs) with three-dimensional confinement of electrons exhibit the drastic change of optical absorption spectra and exotic behaviors which are different from the bulk materials. Hence, the nonlinear optical properties of CSQDs have become a subject of intensive experimental and theoretical studies.[4,12–16] Moreover, nanostructures-based group-III–nitride, especially GaN and InGaN materials, is also a matter of interest due to the wider band-gap characteristic of covering the whole solar spectral region. This exclusive band-gap range is very crucial in fabricating nanoscale solar cell and full-color devices.[17–21] As is well known, the wurtzite $In_xGa_{1-x}N$/GaN structure commonly produces the spontaneous polarization (SP) and piezoelectric (PZ) polarization, which leads to strong built-in electric field (BEF) on the order of MV/cm.[22,23] Many studies show that the BEF has great influence on optical properties of wurtzite $In_xGa_{1-x}N$/GaN nanostructures.[22–25] For instance, the BEF effects on transition energy and optical absorptions in wurtzite $In_xGa_{1-x}N$/GaN quantum well (QW) have been discussed theoretically.[26,27] The exciton states and optical transitions in wurtzite $In_xGa_{1-x}N$/GaN CSQDs have been investigated including the BEF effects.[22,24,28,29]

On the other hand, the linear and nonlinear optical properties of nanostructures are sensitive to many effects such as impurity, material composition, and their size. The impurity effects on the linear, nonlinear, and total optical absorption coefficients (ACs) and refraction index changes (RICs) for the transitions 1s–1p, 1p–1d, and 1d–1f in a GaAs/Al_xGa_{1-x}As spherical QD have been discussed by some authors.[30,31] Ortakaya *et al.*[32] have investigated the linear, nonlinear, and total ACs and RICs in zinc-blende InGaN/GaN multilayer spherical QD with and without impurity. Very recently, the effects of ternary mixed crystal (TMC) and impurity on the linear, nonlinear, and total ACs in GaAs/Al_xGa_{1-x}As multi-shell QD are investigated by Kavruk *et al.*[33] Chi and Shi[27] have reported the influences of TMC and BEF on the linear and nonlinear intersubband optical ACs in $In_xGa_{1-x}N$/$Al_yGa_{1-y}N$ QW. Ghazi and Peter[25] presented a detail study of BEF, impurity, and composition effects on intrasubband transitions between the lowest energy states (1s–1p) in wurtzite InGaN/GaN CSQD by using a variational method. However, variation methods always need appropriately assumed wave functions which will become hard to predict excited states. In contrast, the finite element method (FEM) has proved to be a simple and effective way to solve the electronic states of low-dimensional system.[34–37] In this study, the ground and excited energy state energy values and wave functions are calculated by using the FEM firstly. Then, we investigate the

*Project supported by the National Natural Science Foundation of China (Grant No. 11947414) and the Research Program of Science and Technology at University of Inner Mongolia Autonomous Region, China (Grant No. NJZZ19001).

†Corresponding author. E-mail: xingy@imu.edu.cn

© 2020 Chinese Physical Society and IOP Publishing Ltd

effects of BEF, impurity, TMC, and size on linear, nonlinear, and total ACs and RICs between intersubband 1s–1p, 1p–1d, and 1d–1f transitions for a shallow donor impurity in wurtzite $In_xGa_{1-x}N$/GaN spherical CSQD in detail.

The rest of this paper is organized as follows. In Section 2, the theoretical model is described. In Section 3, the numerical results and discussion are presented, and a brief summary is made in Section 4 finally.

2. Theory

We consider a wurtzite $In_xGa_{1-x}N$/GaN spherical CSQD surrounded by vacuum as shown in Fig. 1.

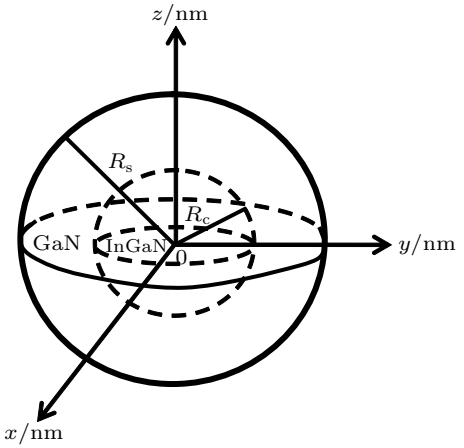


Fig. 1. Schematic structure of $In_xGa_{1-x}N$/GaN spherical CSQD.

The ground and excited energy state energy and wave functions are calculated through solving the Schrödinger equation by using the FEM. The Schrödinger equation of the electron with the BEF for an on-center shallow-donor impurity can be expressed in spherical coordinates. Moreover, we merely consider the simple situation of $m=0$ in this work. Therefore, the radial Schrödinger equation can be written as follows:

$$\begin{aligned} & r^2\frac{\mathrm{d}^2\psi_{n,l}(r)}{\mathrm{d}r^2}+2r\frac{\mathrm{d}\psi_{n,l}(r)}{\mathrm{d}r} \\ & +\left[\frac{2m^*r^2}{\hbar^2}\left(E_{n,l}-V(r)-qFr+\frac{e^2Z}{4\pi\varepsilon_0\varepsilon r}\right)\right. \\ & \left.+l(l+1)\right]\psi_{n,l}(r)=0. \end{aligned} \tag{1}$$

Here, m^* is the effective mass of the electron, E and F are the energy of the system and the BEF of wurtzite material, respectively, $V(r)$ represents the confinement potential of electrons, Z is the impurity charge, and $Z=0$ and $Z=1$ refer to the cases without and with impurity, respectively. The main and angular quantum numbers are expressed by subscripts n and l, r is the electron–impurity distance, ε_0 is the dielectric constant of vacuum, while ε is the relative dielectric constant for the semiconductor material, which can be expressed by the following formula[38]

$$\varepsilon^{\mathrm{InGaN}}=(1-x)\,\varepsilon^{\mathrm{GaN}}+x\varepsilon^{\mathrm{InN}}. \tag{2}$$

Here, x denotes the In-composition. While, the expression of F in Eq. (1) was given by Ref. [22]

$$\begin{cases} F^{\mathrm{InGaN}}=\left|-\dfrac{P_{\mathrm{SP}}^{\mathrm{InGaN}}+P_{\mathrm{PZ}}^{\mathrm{InGaN}}-P_{\mathrm{SP}}^{\mathrm{GaN}}}{\varepsilon_{\mathrm{e}}^{\mathrm{InGaN}}\varepsilon_0}\right|, & r\leqslant R_{\mathrm{c}}, \\ F^{\mathrm{GaN}}\to 0, & r>R_{\mathrm{c}}, \end{cases} \tag{3}$$

where the electronic dielectric constant, the SP and PZ polarization of InGaN (GaN) are denoted as $\varepsilon_{\mathrm{e}}^{\mathrm{InGaN}}$, $P_{\mathrm{SP}}^{\mathrm{InGaN}}$ ($P_{\mathrm{SP}}^{\mathrm{GaN}}$), and $P_{\mathrm{PZ}}^{\mathrm{InGaN}}$ in which the expressions in Ref. [39] has been used. Furthermore, the electrons confinement potential $V(r)$ can be written as

$$V(r)=\begin{cases} 0, & r<R_{\mathrm{c}}, \\ 0.7\left[E_{\mathrm{g}}^{\mathrm{InGaN}}(x)-E_{\mathrm{g}}^{\mathrm{GaN}}\right], & R_{\mathrm{c}}\leqslant r\leqslant R_{\mathrm{s}}, \\ \infty & r>R_{\mathrm{s}}, \end{cases} \tag{4}$$

where R_{c} and R_{s} are the core radius and the outer radius, respectively. In view of the bending factor $b=1.43$ eV,[40,41] the band gap of InGaN $E_{\mathrm{g}}^{\mathrm{InGaN}}$ can be expressed as[41]

$$E_{\mathrm{g}}^{\mathrm{InGaN}}(x)=xE_{\mathrm{g}}^{\mathrm{InN}}+(1-x)E_{\mathrm{g}}^{\mathrm{GaN}}-bx(1-x). \tag{5}$$

The analytical expressions of the linear and nonlinear ACs are described as follows:[42]

$$\begin{aligned} & \alpha^{(1)}(\omega) \\ & =\omega\sqrt{\frac{\mu}{\varepsilon_0\varepsilon}}\frac{\left|M_{ji}\right|^2\sigma_v\hbar\Gamma_0}{(\Delta E-\hbar\omega)^2+(\hbar\Gamma_0)^2}, \end{aligned} \tag{6}$$

$$\begin{aligned} & \alpha^{(3)}(\omega,I) \\ & =-\omega\sqrt{\frac{\mu}{\varepsilon_0\varepsilon}}\left(\frac{I}{2\varepsilon_0 n_{\mathrm{r}}c}\right) \\ & \times\frac{\left|M_{ji}\right|^2\sigma_v\hbar\Gamma_0}{[(\Delta E-\hbar\omega)^2+(\hbar\Gamma_0)^2]^2}\times\left\{4\left|M_{ji}\right|^2\right. \\ & \left.-\frac{\left|M_{jj}-M_{ii}\right|^2[3\Delta E^2-4\Delta E\hbar\omega+\hbar^2(\omega^2-\Gamma_0^2)]}{\Delta E^2+(\hbar\Gamma_0)^2}\right\}. \end{aligned} \tag{7}$$

The total optical absorption coefficient is

$$\alpha^{\mathrm{total}}(\omega,I)=\alpha^{(1)}(\omega)+\alpha^{(3)}(\omega,I). \tag{8}$$

Here, ω is the frequency of an incident photon, $n_{\mathrm{r}}=\sqrt{\varepsilon}$ represents the refractive index, σ_v is the electron density in the present case, Γ_0 is the relaxation rate which is the inverse of relaxation time τ, $\Delta E=E_{ji}=E_j-E_i$ is the intersubband transition energy, moreover, the dipole transition density matrix element between two energy levels can be expressed as $M_{ji}=\left|\langle\psi_j|er|\psi_i\rangle\right|$ The dipole transitions are allowed only between states satisfying the selection rule $\Delta l=\pm 1$.

Similarly, the linear and nonlinear RICs are given by Ref. [42]

$$\frac{\Delta n^{(1)}(\omega)}{n_{\mathrm{r}}}=\frac{\left|M_{ji}\right|^2\sigma_v}{2n_{\mathrm{r}}^2\varepsilon_0}\frac{\Delta E-\hbar\omega}{(\Delta E-\hbar\omega)^2+(\hbar\Gamma_0)^2}, \tag{9}$$

$$\frac{\Delta n^{(3)}(\omega,I)}{n_{\rm r}} = -\frac{|M_{ji}|^2\sigma_v}{4n_{\rm r}^2\varepsilon_0}\frac{\mu cI}{[(\Delta E-\hbar\omega)^2+(\hbar\Gamma_0)^2]^2} \times\left\{4(\Delta E-\hbar\omega)|M_{ji}|^2-\frac{|M_{jj}-M_{ii}|^2}{\Delta E^2+(\hbar\Gamma_0)^2} \times\{(\hbar\Gamma_0)^2(2\Delta E-\hbar\omega)-(\Delta E-\hbar\omega) \times[\Delta E(\Delta E-\hbar\omega)-(\hbar\Gamma_0)^2]\}\right\}. \quad (10)$$

The total refractive index change is

$$\frac{\Delta n^{\rm total}(\omega,I)}{n_{\rm r}} = \frac{\Delta n^{(1)}(\omega)}{n_{\rm r}} + \frac{\Delta n^{(3)}(\omega,I)}{n_{\rm r}}. \quad (11)$$

3. Numerical results and discussion

In this section, the numerical calculations of optical absorption for a wurtzite $In_xGa_{1-x}N$/GaN spherical CSQD are carried out. The following parameters are used in our calculations: $m^*_{\rm InN}=0.10m_0$, $m^*_{\rm GaN}=0.19m_0$, $E_{\rm g}^{\rm InN}=0.78$ eV, $E_{\rm g}^{\rm GaN}=3.42$ eV, $\varepsilon^{\rm InN}=15$, $\varepsilon^{\rm GaN}=9.6$, $\sigma_v=3\times10^{22}$ m^{-3}, and $\tau=200$ fs, and other material parameters are the same as those in Ref. [36].

Firstly, in order to investigate the impurity effects, we plot the linear, nonlinear, and total ACs and RICs for 1s–1p, 1p–1d, and 1d–1f transitions each as a function of the incident photon energy in a $In_{0.5}Ga_{0.5}N$/GaN CSQD with $Z=0$ and $Z=1$ in Fig. 2, without considering the BEF. In Fig. 2(a), it appears that the presence of the impurity causes the linear, nonlinear, and total ACs resonant peaks to be blue-shifted significantly for all transitions. This is because the attractive Coulomb potential leads the eigenenergy to decrease, and this effect decreases as the levels go up, so the transition energy between the levels in the case with impurity is larger than that in the case without impurity case. In addition, this shift is more pronounced in transitions between lower levels, *i.e.*, it is about 21 meV for 1s–1p, 7 meV for 1p–1d, and 4 meV for 1d–1f, respectively. The reason can be explained as follows: the electron is more strongly localized near the impurity due to the attractive Coulomb potential, and the effect becomes much more effective on lower level. The RIC is also an important parameter for the investigation of optical properties. As can be seen in Fig. 2(b), the linear and third-order nonlinear RICs are always opposite to each other and the nonlinear term is large enough to affect the total RIC. Further, there exist two distinct regions in terms of the photon energy. The first region is between two extreme values of the total RIC where $\mathrm{d}(\Delta n)/\mathrm{d}\omega<0$, and the photon is very strongly absorbed. So this region is defined as absorption band, also, is called anomalous dispersion region. The other region is outside the anomalous region, which is called the normal dispersion region and the total RIC increases as the photon energy increases, that is $\mathrm{d}(\Delta n)/\mathrm{d}\omega>0$. It is also found that the linear, nonlinear, and total RIC curves intersect to the horizontal axis at the resonance photon energy, and the frequency of resonance photon energy is the resonance frequency of the system. It is obviously shown that in all transitions, the resonant peak values of RIC in the case with impurity shift towards the higher photon energy (blue shift). This is because the presence of the impurity leads the electron transition energy to increase. As a result, it can be said that the impurity affects the ACs and RICs dramatically.

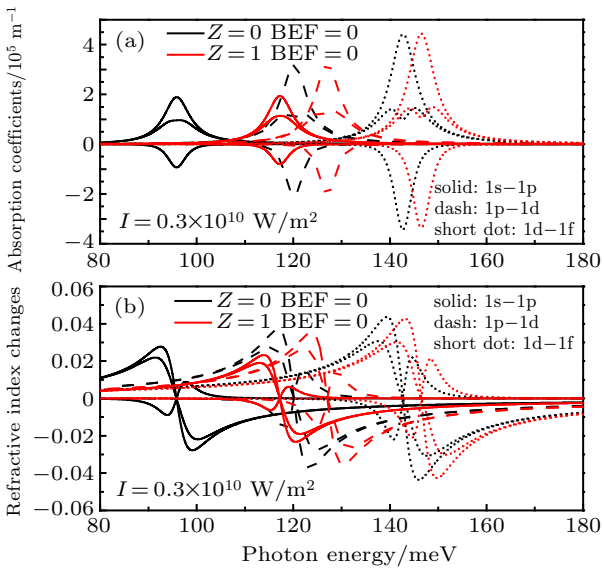


Fig. 2. (a) Linear, nonlinear, and total ACs and (b) RICs for 1s–1p, 1p–1d, and 1d–1f transitions as a function of incident photon energy in $In_{0.5}Ga_{0.5}N$/GaN (5 nm/3 nm) CSQD with and without impurity.

The effects of BEF on the ACs and RICs for 1s–1p, 1p–1d, and 1d–1f transitions in $In_{0.5}Ga_{0.5}N$/GaN CSQD without impurity are shown in Fig. 3. First, we can clearly find that the linear, nonlinear, and total ACs and RICs resonant peaks for all transitions shift towards the higher photon energy when considering the BEF, and the blue shift more decreases for the transitions between higher states. The physical origin is that the BEF tilts electronic potential and raises eigenenergy to a higher level. The transition energy E_{ji} increases with the generation of BEF and the BEF effect decreasing as the level goes up. Second, it can be seen from Fig. 3(a) that the amplitudes of the total ACs significantly increase with the BEF effect strengthening. According to Eqs. (6)–(8), the total optical ACs are proportional to $E_{ji}\cdot(|M_{ij}|^2-|M_{ij}|^4)$. Here, in contrast to the increase of the transition energy E_{ji}, the dipole moment matrix element $|M_{ji}|$ decreases as the overlap integral of election wave function reduces when considering the BEF. The competition between the two factors determines the variation trend of the amplitudes of the total ACs, and the influence of E_{ji} turns out to be more significant. As far as the linear, nonlinear, and total RICs are concerned, their amplitudes exhibit an obviously decrease when the BEF is considered. This is in accordance with Eqs. (9)–(11) and the reason for this variation is similar to that in Fig. 3(a), but the influence of the dipole moment matrix element is more dominant. Therefore, to ob-

tain desired ACs and RICs, the effect of BEF should be taken into account.

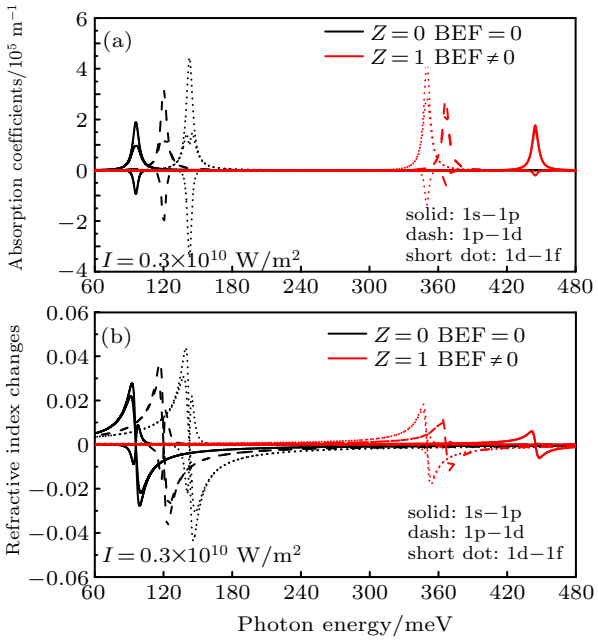


Fig. 3. (a) Linear, nonlinear, and total ACs and (b) RICs for 1s–1p, 1p–1d, and 1d–1f transitions each as a function of incident photon energy in $In_{0.5}Ga_{0.5}N$/GaN (5 nm/3 nm) CSQD with and without the BEF.

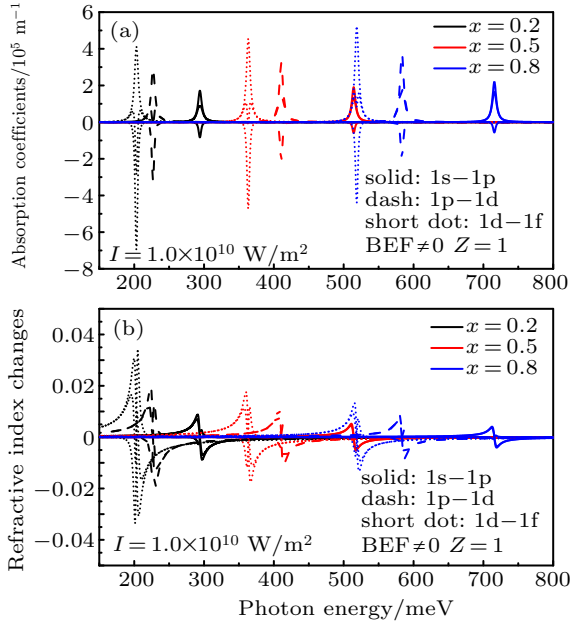


Fig. 4. (a) Linear, nonlinear, and total ACs and (b) RICs for 1s–1p, 1p–1d, and 1d–1f transitions each as a function of incident photon energy for $x=0.2$, 0.5, 0.8 in $In_xGa_{1-x}N$/GaN (5 nm/3 nm) CSQD with impurity and BEF.

To investigate the effects of the TMC on the optical properties, in Fig. 4 we present the dependence of the linear, nonlinear, and total ACs and RICs on photon energy for $x=0.2$, 0.5, 0.8 in a wurtzite $In_xGa_{1-x}N$/GaN CSQD with the impurity and BEF, showing that the increasing of x value leads the resonant peaks to be blue-shifted for 1s–1p, 1p–1d, and 1d–1f transitions. These behaviors originate from the effects of TMC on the confinement potential $V(r)$ and the BEF. As In-composition x increases, the electron is more strongly localized inside the dot due to the enhancement of the BEF and $V(r)$, which causes the initial and final energy levels to be largely separate. So the electron transition energy increases with the value of x increasing. At the same time, it is also noted from the figure that the amplitudes of the total ACs increase with the value of x increasing, while for the total RICs the amplitudes decrease and the slopes change their sign at $E_{ji}=\hbar\omega$. Furthermore, the dipole moment matrix element is diminished by increasing the value of x. The competition between the transition energy and the dipole moment matrix element leads to the change as described above. These results reveal that the optical properties of the CSQD can be tuned to the suitable level by adjusting composition x.

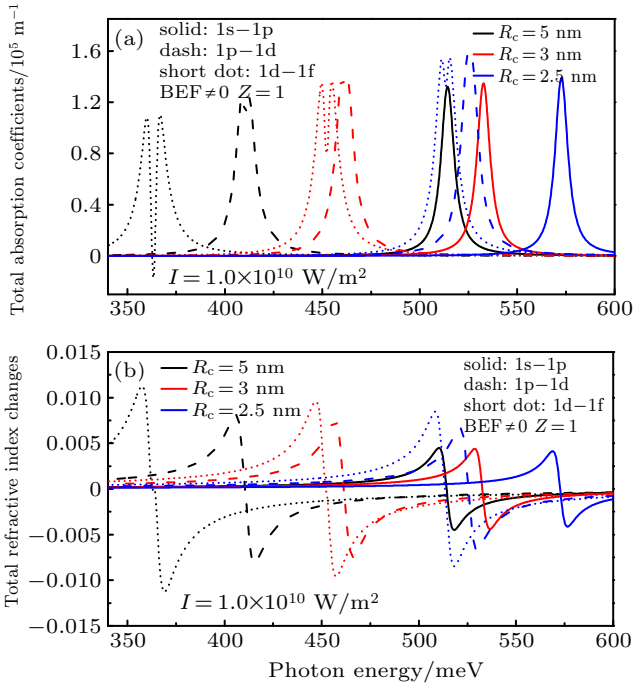


Fig. 5. (a) Total ACs and (b) RICs *versus* incident photon energy for 1s–1p, 1p–1d, and 1d–1f transitions for $R_c=2.5$, 3, and 5 nm in $In_{0.5}Ga_{0.5}N$/GaN (R_c/3 nm) CSQDs with the impurity and the BEF.

Figure 5 shows the total ACs and RICs *versus* the incident photon energy of a wurtzite $In_{0.5}Ga_{0.5}N$/GaN CSQD for core radius $R_c=2.5$ nm, 3 nm, and 5 nm with the impurity and the BEF, and the shell thickness is fixed at 3 nm. We can clearly see that the total ACs and RICs for all transitions exhibit an obvious red shift when the core radius increases. The reason is attributed to the reduction of transition energy, which is induced by weakening electron confinement. From the figure, it is observed that the amplitudes of the total ACs decrease while the total RICs increase as core radius increases. This result can be explained by the following fact: the increasing of the core radius weakens the quantum confinement, which leads the transition energy to decrease and the dipole matrix element to be enhanced. The competition between the two factors results in the above result. For the total AC, the tran-

sition energy is more dominant in the case of large core radius, whereas the dipole matrix element is more dominant in the case of small core radius. But the conclusion is contrary to each other for the total RIC. This tendency has been confirmed by the result obtained in Refs. [38,42]. We also find that the quantum size effect is much stronger in the transitions between higher levels. This is because the excited state is more sensitively dependent on the quantum confinement effect and has a remarkable influence on the transition energy. Thus, these results indicate that the optical absorption can be finely tuned by adjusting the core size.

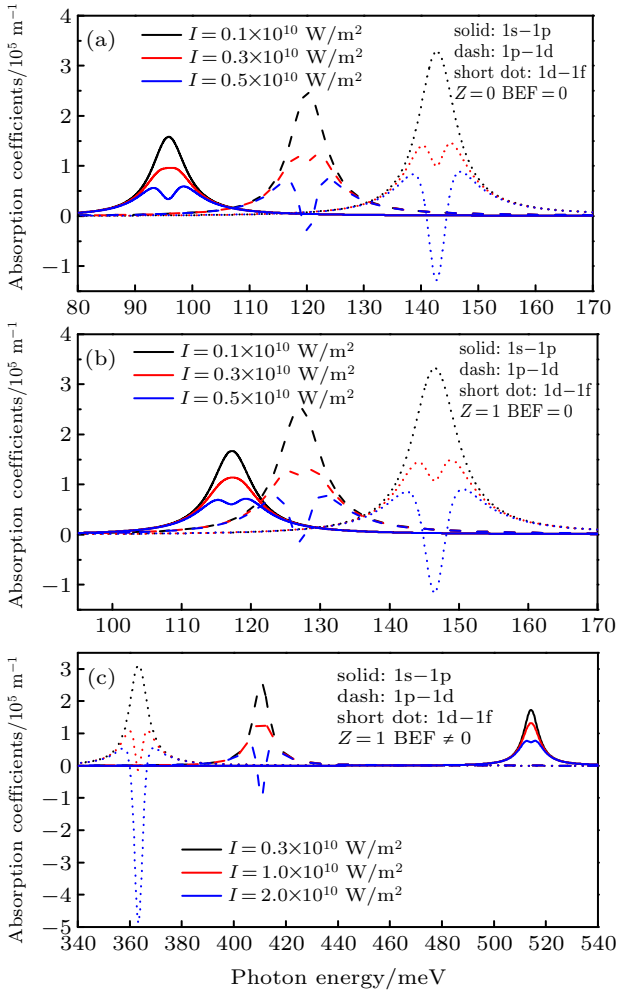


Fig. 6. Total ACs *versus* incident photon energy of 1s–1p, 1p–1d, and 1d–1f transitions for various values of the incident optical intensity I in $In_{0.5}Ga_{0.5}N$/GaN (5 nm/3 nm) CSQDs (a) with $Z = 0$ and BEF = 0, (b) with $Z = 1$ and BEF = 0, and (c) with $Z = 1$ and BEF $\neq 0$.

To illustrate the effect of the incident optical intensity, we plot the total ACs of $In_{0.5}Ga_{0.5}N$/GaN CSQD *versus* incident photon energy for various values of the incident optical intensity I ($I = 0.1\times10^{10}$ W/m^2, 0.3×10^{10} W/m^2, 0.5×10^{10} W/m^2, 1.0×10^{10} W/m^2, and 2.0×10^{10} W/m^2) in Fig. 6. It can be seen from the figure that with the increase of I, the amplitudes of total ACs decrease significantly for 1s–1p, 1p–1d, and 1d–1f transitions no matter whether the impurity and BEF are considered. This is because the third-order nonlinear ACs have a noticeable contribution to the total ACs since the linear ACs are independent of incident optical intensity and the nonlinear ACs have a negative increase as intensity increases. The higher the incident optical intensity I, the larger the contribution of the nonlinear term will be. When I exceeds a threshold value I_t, the splitting of the total AC peak is observed, *i.e.*, the absorption saturation occurs. With the value of I increasing, the newly formed minimum of AC becomes negative value. This important characteristic is related to the design of CSQD as a laser amplifier. Moreover, figures 6(a) and 6(b) reveal that the threshold value I_t increases in the case with impurity, which indicates the saturation of total AC is more sensitive in the case without the impurity. For example, the saturation for 1s–1p transition begins to occur around 0.31×10^{10} W/m^2 in the case without impurity and at 0.38×10^{10} W/m^2 in the case with impurity. So we are more interested in this property, which may be applied to the design of optoelectronic devices. In addition, figure 6(c) shows that the threshold value I_t is very strongly dependent on the presence of BEF. The saturation occurs at a larger incident optical intensity, *i.e.*, it is about 1.75×10^{10} W/m^2 for 1s–1p transition. It is also noticed that the threshold value I_t is smaller for the transitions between higher levels. In combination with the plot of Figs. 4 and 5, we can also conclude that the saturation of ACs becomes more susceptible with the value of x decreasing or the core radius increasing.

4. Conclusions

In this work, we investigated the linear, nonlinear, and total optical ACs and RICs of 1s–1p, 1p–1d, and 1f–1d transitions in wurtzite $In_xGa_{1-x}N$/GaN spherical CSQD with a shallow donor impurity by using density matrix approach, the BEF effect is included. The finite element method is used to calculate the energy and corresponding wave functions. The results reveal that the BEF has a great influence on the linear, nonlinear, and total ACs and RICs. The presence of impurity leads to the resonant peaks of the ACs and RICs to be blue-shifted for all transitions, especially for 1s–1p transition. It is also found that the resonant peaks of the ACs and RICs present obviously a blue shift with the increase of the In-composition. Moreover, the ACs and RICs are strongly affected by the CSQD size and the resonant peaks experience a red shift as the core radius increases. In addition, the saturation of total ACs is more sensitive in the case without the impurity than in the case with the impurity, and the occurrence of saturation requires a larger incident optical intensity when considering the BEF. We expect the present work will be able to conduce to theoretical and experimental research on the optical properties of the spherical CSQDs.

References

[1] Ji L W, Su Y K, Chang S J, Liu S H, Wang C K, Tsai S T, Fang T H, Wu L W and Xue Q K 2003 *Solid-State Electron.* **47** 1753
[2] Yu J S, Slivken S, Evans A, David J and Razeghi M 2003 *Appl. Phys. Lett.* **82** 3397
[3] Zhao F, Lv X, Majumdar A and Shi Z 2004 *Appl. Phys. Lett.* **84** 1251
[4] Ji L W, Young S J, Liu C H, Water W, Meen T H and Jywe W Y 2008 *J. Cryst. Growth* **310** 2476
[5] Asgari A and Razi S 2010 *Opt. Express* **18** 14604
[6] Yanover D, Čapek R K, Brusilovski A R, Vaxenburg R, Grumbach N, Maikov G I, Solomeshch O, Sashchiuk A and Lifshitz E 2012 *Chem. Mater.* **24** 4417
[7] Jahangir S, Pietzonka I, Strassburg M and Bhattacharya P 2014 *Appl. Phys. Lett.* **105** 111117
[8] Tsai C L 2016 *J. Lumin.* **174** 36
[9] Zhang L, Teng C H, Ku P C and Deng H 2016 *Appl. Phys. Lett.* **108** 153102
[10] Saravanamoorthy S N, Peter A J and Lee C W 2017 *Chem. Phys.* **483–484** 1
[11] Wu Q Q, Cao F, Kong L M and Yang X Y 2019 *Chin. Phys. B* **28** 118103
[12] Damilano B, Grandjean N, Dalmasso S and Massies J 1999 *Appl. Phys. Lett.* **75** 3751
[13] Lu L L, Xie W F and Hassanabadi H 2011 *J. Appl. Phys.* **109** 063108
[14] Yakar Y, Çakır B and Özmen A 2010 *Opt. Commun.* **283** 1795
[15] Cristea M, Radu A and Niculescu E C 2013 *J. Lumin.* **143** 592
[16] She Y C, Luo T T, Zhang W X, Ran M W and Wang D L 2016 *Chin. Phys. B* **25** 014202
[17] Jani O, Ferguson I, Honsberg C and Kurtz S 2007 *Appl. Phys. Lett.* **91** 132117
[18] Gorji N E, Movla H, Sohrab F, Hosseinpour A, Rezaei M and Babaei H 2010 *Physica E* **42** 2353
[19] Ren Z W, Chao L, Chen X, Zhao B J, Wang X F, Tong J H, Zhang J, Zhuo X J, Li D W, Yi H X and Li S T 2013 *Opt. Express* **21** 7118
[20] Movla H 2016 *Optik* **127** 4799
[21] Afkir N B, Feddi E, Dujardin F, Zazoui M and Meziane J 2018 *Physica B* **534** 10
[22] Shi J J and Gan Z Z 2003 *J. Appl. Phys.* **94** 407
[23] Shi J J, Xia C X, Wei S Y and Liu Z X 2005 *J. Appl. Phys.* **97** 083705
[24] Zhang M and Shi J J 2011 *Superlattices Microstruct.* **50** 529
[25] Ghazi H E and Peter A J 2015 *Physica B* **470–471** 64
[26] Guo L C, Wang X L, Xiao H L and Wang B Z 2007 *J. Cryst. Growth* **298** 522
[27] Chi Y M and Shi J J 2008 *J. Lumin.* **128** 1836
[28] Xia C X and Wei S Y 2005 *Phys. Lett. A* **346** 227
[29] Xia C X and Wei S Y 2006 *Phys. Lett. A* **359** 161
[30] Özmen A, Yakar Y, Çakır B and Atav U 2009 *Opt. Commun.* **282** 3999
[31] Çakır B, Yakar Y and Özmen A 2012 *J. Lumin.* **132** 2659
[32] Ortakaya S, Kirak M and Guldeste A 2017 *J. Nonlinear Opt. Phys. Mater.* **26** 1750035
[33] Kavruk A E, Sahin M and Koc F 2013 *J. Appl. Phys.* **114** 183704
[34] Zhang L, Yu Z, Yao W, Liu Y and Ye H 2010 *Superlattices Microstruct.* **48** 434
[35] Jbara A S, Othaman Z and Saeed M A 2016 *Chin. Phys. B* **25** 057801
[36] Liu W H, Qu Y and Ban S L 2017 *Superlattices Microstruct.* **102** 373
[37] Cao X M, Liu W H, Yang X C, Qu Y and Xing Y 2019 *Mod. Phys. Lett. B* **33** 1950367
[38] Ghazi H E, Jorio A and Zorkani I 2014 *J. Optoelectron. Adv. Mater.* **16** 1242
[39] Ambacher O, Majewski J, Miskys C, Link A, Hermann M, Eickhoff M, Stutzmann M, Bernardini F, Fiorentini V, Tilak V, Schaff B and Eastman L F 2002 *J. Phys.: Condens. Matter* **14** 3399
[40] Wu J, Walukiewicz W, Yu K M, Ager J W, Haller E E, Lu H and Schaff W J 2002 *Appl. Phys. Lett.* **80** 4741
[41] Wu J Q 2009 *J. Appl. Phys.* **106** 011101
[42] Rezaei G, Vahdani M R K and Vaseghi B 2011 *Physica B* **406** 1488